Theranostic Approach for Metastatic Pigmented Melanoma Using ICF15002, a Multimodal Radiotracer for Both PET Imaging and Targeted Radionuclide Therapy[1]

CrossMark

Latifa Rbah-Vidal [*,†], Aurélien Vidal [*,‡], Emilie M.F. Billaud [*], Sophie Besse [*], Isabelle Ranchon-Cole [§], Florence Mishellany [¶], Yann Perrot [#], Lydia Maigne [#], Nicole Moins [*], Jean-Luc Guerquin-Kern [**], Françoise Degoul [*], Jean-Michel Chezal [*], Philippe Auzeloux [*] and Elisabeth Miot-Noirault [*]

[*]UMR 990 INSERM/Université d'Auvergne, F-63005 Clermont-Ferrand, France; [†]UMR 892 INSERM/6299 CNRS/Université de Nantes, F-44007 Nantes, France; [‡]Arronax, CS 10112, F-44817 Saint Herblain Cedex, France; [§]UMR 1107 INSERM/Université d'Auvergne, Equipe Biophysique Neurosensorielle, F-63000 Clermont-Ferrand, France; [¶]Centre Jean Perrin, Laboratoire d'anatomo-pathologie, F-63011 Clermont-Ferrand, France; [#]CNRS/IN2P3/Université Blaise Pascal, Laboratoire de Physique Corpusculaire, F-63000 Clermont-Ferrand, France; [**]INSERM, U1196, F-91405, Orsay, France

Abstract

PURPOSE: This work reports, in melanoma models, the theranostic potential of ICF15002 as a single fluorinated and iodinated melanin-targeting compound. *METHODS:* Studies were conducted in the murine syngeneic B16BL6 model and in the A375 and SK-MEL-3 human xenografts. ICF15002 was radiolabeled with fluorine-18 for positron emission tomography (PET) imaging and biodistribution, with iodine-125 for metabolism study, and iodine-131 for targeted radionuclide therapy (TRT). TRT efficacy was assessed by tumor volume measurement, with mechanistics and dosimetry parameters being determined in the B16BL6 model. Intracellular localization of ICF15002 was characterized by secondary ion mass spectrometry (SIMS). *RESULTS:* PET imaging with [^{18}F]ICF15002 evidenced tumoral uptake of $14.33 \pm 2.11\%$ID/g and $4.87 \pm 0.93\%$ID/g in pigmented B16BL6 and SK-MEL-3 models, respectively, at 1 hour post inoculation. No accumulation was observed in the unpigmented A375 melanoma. SIMS demonstrated colocalization of ICF15002 signal with melanin polymers in melanosomes of the B16BL6 tumors. TRT with two doses of 20 MBq [^{131}I]ICF15002 delivered an absorbed dose of 102.3 Gy to B16BL6 tumors, leading to a significant tumor growth inhibition [doubling time (DT) of 2.9 ± 0.5 days in treated vs 1.8 ± 0.3 in controls] and a prolonged median survival (27 days vs 21 in controls). P53S15 phosphorylation and P21 induction were associated with a G2/M blockage, suggesting mitotic catastrophe. In the human SK-MEL-3 model, three doses of 25 MBq led also to a DT increase (26.5 ± 7.8 days vs 11.0 ± 3.8 in controls) and improved median survival (111 days vs 74 in controls). *CONCLUSION:* Results demonstrate that ICF15002 fulfills suitable properties for bimodal imaging/TRT management of patients with pigmented melanoma.

Neoplasia (2017) 19, 17–27

Introduction

Advanced melanoma has historically been associated with a poor prognosis, a median overall survival (OS) of 8 to 10 months, and a 5-year survival rate of 10% [1]. Prior to 2011, the first-line treatment of metastatic disease was dacarbazine, with innovative strategies being limited to interferon-α2b for adjuvant therapy or high-dose interleukin-2. Since 2011, new agents have been approved for the treatment of metastatic melanoma disease such as anti-CTLA4 monoclonal antibody (ipilimumab) as well as BRAF inhibitors (vemurafenib, dabrafenib, or trametinib) in patients harboring BRAFV600 mutations. More recently, additional inhibitors for checkpoint immunosuppression emerged with anti-PD-1–based approaches producing response rates above 50% during more than 1 year when administered in combination with anti-CTL4 [2–6]. Although these treatments led to considerably improved survival benefits for patients, tumor molecular heterogeneity is rapidly being evidenced as a complicating factor in the efficacy of targeted therapies, the durability of responses, and the development of drug resistance [7]. Some patients with metastatic melanoma treated with chemo-, targeted, or immunotherapies showed mixed responses to treatment. Whereas some lesions underwent responses to therapy, even complete regression, other lesions in the same patient continued to progress, or in some cases, new lesions developed, indicating drug resistance. Moreover, adverse effects have been observed for both immunotherapy and BRAF inhibitors: the use of BRAF inhibitors was associated to cutaneous side effects, including secondary tumors such as squamous cell carcinoma, keratoacanthoma, and also cutaneous toxicities (rash, photosensitivity reactions, alopecia) [8–10]. Therefore, it appears that one interesting approach for a long-term control of melanoma would involve a combination of targeted approaches. An intrinsic property of melanoma is the presence of melanin in 20% to 30% of metastases, making it a very attractive target. Many studies highlighted melanin-specific benzamide derivative compounds to offer strategies for both nuclear medicine imaging and internal radionuclide therapy of disseminated pigmented melanoma with a high selectivity [11–14]. For melanoma single photon emission computed tomography (SPECT) imaging, N-(2-diethylaminoethyl)-4-iodobenzamide and N-(2-diethylaminoethyl)-2-iodobenzamide (BZA2) have been radiolabeled with iodine-123 and evaluated in phase II and, for the latter, in multicentric phase III clinical studies, suggesting that such radiotracers could be used to select patients with pigmented metastases, allowing them to be eligible to melanin-targeted therapies [14,15]. For melanoma positron emission tomography (PET) imaging, several fluorinated arylcarboxamide derivatives were developed, such as [18F]-6-fluoro-N-[2-(diethylamino)ethyl]pyridine-3-carboxamide ([18F]MEL050 or [18F]ICF01006). In preclinical studies, this radiotracer demonstrated promising results in primary and metastatic melanoma models, with superior contrast and specificity in pigmented-melanoma models [16]. For melanin-targeted radionuclide therapy (TRT), many arylcarboxamide derivatives such as [131I]MIP-1145 and [131I]ICF01012 exhibited a strong efficacy in murine and human melanoma xenografts [17–19]. A first clinical study using the analogue [131I]BA52 demonstrated promising survival benefits and favorable dosimetry in patients with metastases, strengthening the high potential of this class of compounds for TRT of melanotic tumors [20].

Taken together, these results prompted us to initiate a theranostic approach using a unique arylcarboxamide scaffold which can be radiolabeled either with fluorine-18 for PET selection of melanin-positive patient subgroup eligible to TRT or with iodine-131 for therapy.

Among the large variety of arylcarboxamides evaluated, [18F]ICF15002 emerged as the most promising compound with high accumulation in tumors and rapid elimination from nontarget organs [21,22]. Next step was then to demonstrate the usefulness of ICF15002 for theranostic management in both human and murine melanoma preclinical models. We investigated here PET imaging and distribution of [18F]ICF15002, metabolism studies with [125I]ICF15002, and radiotherapeutic efficacy of [131I]ICF15002. For TRT applications, mechanistic and dosimetric parameters have also been determined.

Materials and Methods

Synthesis of ICF15002

The structure of N-(12-ethyl-1-fluoro-3,6,9-trioxa-12-azatetradecan-14-yl)-6-iodoquinoxaline-2-carboxamide (ICF15002) is shown in Supplementary Figure 1A. Synthesis of ICF15002 was performed as already described [21,22].

Radiolabeling of [131I]ICF15002 and [125I]ICF15002

Synthesis of tributylstannane precursor ICF15060 is detailed in supplementary data. To a solution of ICF15060 (50 µl, 1 mg/ml in EtOH) were successively added, in a sealed vial, [131I]NaI (1517 MBq) or [125I]NaI (304 MBq), an aqueous HCl solution (50 µl, 1 N for 131I-radiolabeling or 0.5 N for 125I-radiolabeling), and an aqueous solution of Chloramine-T monohydrate (20 µl, 1 mg/ml). The reaction mixture was left at room temperature for 1 hour (vortexed every 20 minutes). The resulting solution was quenched by addition of 1 N aqueous NaOH solution (100 µl for 131I-radiolabeling or 25 µl for 125I-radiolabeling) and aqueous sodium metabisulfite solution (10 µl, 20 mg/ml). The mixture was purified by semipreparative HPLC [Waters Symmetry Prep C18 column (300 × 7.8 mm, porosity 7 µm); MeOH/H_2O (0.2% NH_4OH) 70:30 to 100:0 v/v linear gradient in 15 minutes then 70:30 v/v isocratic during 15 minutes] at a flow rate of 1.2 ml/min. The product peak was collected (retention time 20.04 minutes) and evaporated to dryness. The formulation was achieved in EtOH/saline 05:95 v/v.

Radiolabeling of [18F]ICF15002

Please refer to [22].

Cell Lines and In Vivo Graft for Melanoma Models. The syngenic melanoma cell line B16BL6 was obtained from Dr. Fidler Laboratories (Texas University, USA). SK-MEL-3 and amelanotic A375 melanoma lines were obtained from the American Type Culture Collection. B16BL6 cells were cultured as published [16]. SK-MEL-3 cells were maintained in McCoy's 5A medium (Invitrogen) containing 15% FBS. A375 cells were maintained in Dulbecco's modified Eagle's medium (Invitrogen) supplemented with 10% fetal bovine serum (Sigma). All cells were grown in a humidified incubator at 37°C/5% CO_2.

For *in vivo* xenograft melanoma models, all protocols were conducted in accordance with the 2010/63/UE Directive after approval by the institutional review board C2E2A from Auvergne Region (Authorization CE 115-12 and CE 116-12). The murine graft was performed by subcutaneous injection of 3×10^5 B16BL6 cells in PBS (0.1 ml) on the right shoulder of male C57BL6/J mice, 6 weeks old (Charles River). This model exhibited spontaneous pulmonary dissemination from primary melanoma site.

For human xenografts, 3×10^6 SK-MEL-3 (pigmented line) or A375 (nonpigmented line) cells in PBS (0.1 ml) were subcutaneously injected on the right shoulder of female Swiss *nu/nu* mice, 6 weeks old (Charles River). Experiments started when tumors were measurable, *i.e.*, around day 15 for murine model and day 30 for human models.

For melanoma lung colonies used for secondary ion mass spectroscopy analysis, 3×10^5 B16BL6 cells in PBS (0.1 ml) were intravenously injected to male C57BL6/J mice, 6 weeks old (Charles River), and experiments were performed at day 12 after inoculation.

Distribution of Radiolabeled ICF15002 in Tumor and Tissues and In Vivo Metabolism

When tumors evidenced a diameter of approximately 8 mm, distribution of [^{18}F]ICF15002 was undertaken in the three melanoma xenograft models (pigmented B16BL6 murine and SK-MEL-3 human model, and amelanotic A375 human model) by both *in vivo* imaging (*n* = 3-8 animals/group) and organ counting (*n* = 3-6 animals/group). Animals were injected with 9 to 12 MBq of [^{18}F]ICF15002 in a volume of 0.15 ml and examined at 30 minutes, 1 hour, and 2 hours after injection. For biodistribution study, tumor and tissues were harvested and weighed, and their radioactivity was counted using a Wallac 1480 automated calibrated γ-counter (Perkin- Elmer, Waltham, MA) with a 400 to 600 keV energy window and decay correction. Results were expressed as %ID/g.

For *in vivo* PET imaging, whole-body scans were acquired using a small-animal device (eXplore Vista, GE Healthcare). Acquisition (30 minutes duration, 2 bed positions) was performed with a 250 to 700 keV energy window set and 6-nanosecond coincidence time window. Images were reconstructed using a two-dimensional ordered subset expectation maximization (Fourier rebinning) method including corrections for scanner dead time, scatter radiations and randoms. Tracer uptake was quantified from *in vivo* scans with eXplore Vista software package (GE Healthcare), with volume of interest delineated over tumor and muscle (considered as background): the mean counts per pixel per minute per ml of tissue were obtained and expressed as percentage of injected dose per g (%ID/g). *In vivo* tumor to background ratio was calculated by dividing the %ID/g value of tumor by the %ID/g value of muscle.

For metabolism studies, [^{125}I]ICF15002 was IV administered to B16BL6-bearing mice (*n* = 24 mice with 4 animals per time point). Animals were injected with 2.2 MBq of [^{125}I]ICF15002 and sacrificed by CO_2 inhalation at selected time points (1, 3, 6, 24, and 72 hours and 10 days), with tumor, tissues, urine, and feces being collected. After methanol extraction (yields: 50%-90% for blood, liver and kidneys; 20%-63% for tumor and eyes), samples were analyzed by HPLC and metabolites quantified. For identification, retention times were compared with those of nonradioactive counterparts [23].

Intracellular Localization of ICF15002 in Melanoma Micrometastases by Secondary Ion Mass Spectrometry Analysis (SIMS). SIMS was performed on small lung melanoma colonies (mimicking lung micrometastases) from mice injected with nonradiolabeled ICF15002 (0.1 μmol/mice by IV route) using a NanoSIMS-50 Ion Microprobe (CAMECA). At 1 hour after ICF15002 administration, small lung samples with melanoma deposits were isolated and fixed by slam freezing on an LN2-precooled metal mirror. Samples were dehydrated by freeze drying starting at –110°C to –10°C and embedded in Spurr resin. Serial sections of 0.4 μm thickness were placed on stainless steel holders for SIMS analysis or on glass slides for light microscopy observation. The primary ion beam was generated by a cesium source and accelerated to get impact energy of 16 keV. For typical experiments, the probe size was 100 nm in diameter (defined as 16%-84% rise distance of the signal intensity), with a current of 1.5 pA. The probe scanned the surface of the sample in a 256×256 pixel raster. Images were acquired in two sequential series ($^{12}C^{14}N^-$, $^{31}P^-$, and $^{127}I^-$ then ^{12}C $^{14}N^-$, $^{32}S^-$, and $^{127}I^-$) and analyzed with ImageJ.

Assessment of [^{131}I]ICF15002 TRT in Murine and Human Melanoma Models: Tumor Growth, Doubling Time (DT), and Survival

TRT experiments with [^{131}I]ICF15002 were undertaken in both B16BL6 murine and SK-MEL-3 human models. For both models, the thyroid uptake was blocked with potassium iodide (administration *per os* 3 days before TRT). First of all, the antitumor activity of [^{131}I]ICF15002 was evaluated and extensively characterized in the highly pigmented B16BL6 melanoma model, which is recognized to exhibit spontaneous pulmonary dissemination. B16BL6 melanoma–bearing mice were submitted to two intravenous injections of 20 MBq, at day 7 and day 11 post inoculation (p.i.).

To assess the relevance of melanin TRT in human melanoma, the antitumor efficacy of [^{131}I]ICF15002 was also determined in SK-MEL-3 xenografts, which exhibit lower amount of melanin. In this model, two protocols were assessed: 1) two IV injections of 25 MBq, at day 33 and day 40 and 2) three IV injections of 25 MBq, at days 33, 40, and 47.

For all models, tumor volume (TV) was calculated as follows from two-dimensional caliper measurements being performed twice a week.

$$TV \ (mm^3) = L \times W^2/2$$ where L (length) and W (width) are expressed in mm.

TV values were averaged within each group at each time point. DT was also determined to evaluate tumor growth.

Animals were also monitored for body weight with daily survival monitoring and were euthanized by CO_2 when end points were evidenced.

Extensive Characterization of TRT with [^{131}I]ICF15002 in B16BL6 Model: Dosimetry, Histology, and Molecular Studies

To further characterize TRT, mechanistic studies as well as dosimetry were assessed in B16BL6 model.

For mechanistic studies, eight additional B16BL6-bearing mice were used: *n* = 3 controls and 5 animals treated as described above with two intravenous injections of 20 MBq at day 7 and day 11 p.i. At 24 hours, 72 hours, and 10 days after TRT, eyes and skin were removed for histology and tumors for mechanistic studies. Blood was also collected by cardiac puncture on anesthetized animals, and leukocyte numbers were quantified by kit (Leuko-tic, Bioanalytic, France) according to the manufacturer's instructions.

VEGF expression was assessed by an ELISA kit (Raybiotech). For WB, proteins were extracted from 10 mg of crushed tumor in lysis buffer (6 M urea, 5 mM NaF, 2.5 mM sodium pyrophosphate, 1 mM EDTA, 0.5% Triton X100, 1 mM activated sodium orthovanadate, 1 protease inhibitors) and loaded (30 μg) onto 12.5% sodium dodecyl sulfate polyacrylamide gel electrophoresis. Proteins were separated, transferred to nitrocellulose membranes (Millipore), stained with Ponceau red, and probed with anti-P53S15 (Cell Signaling, Ozyme), anti-P21 (Santa Cruz), and anti-GAPDH (Santa Cruz). The
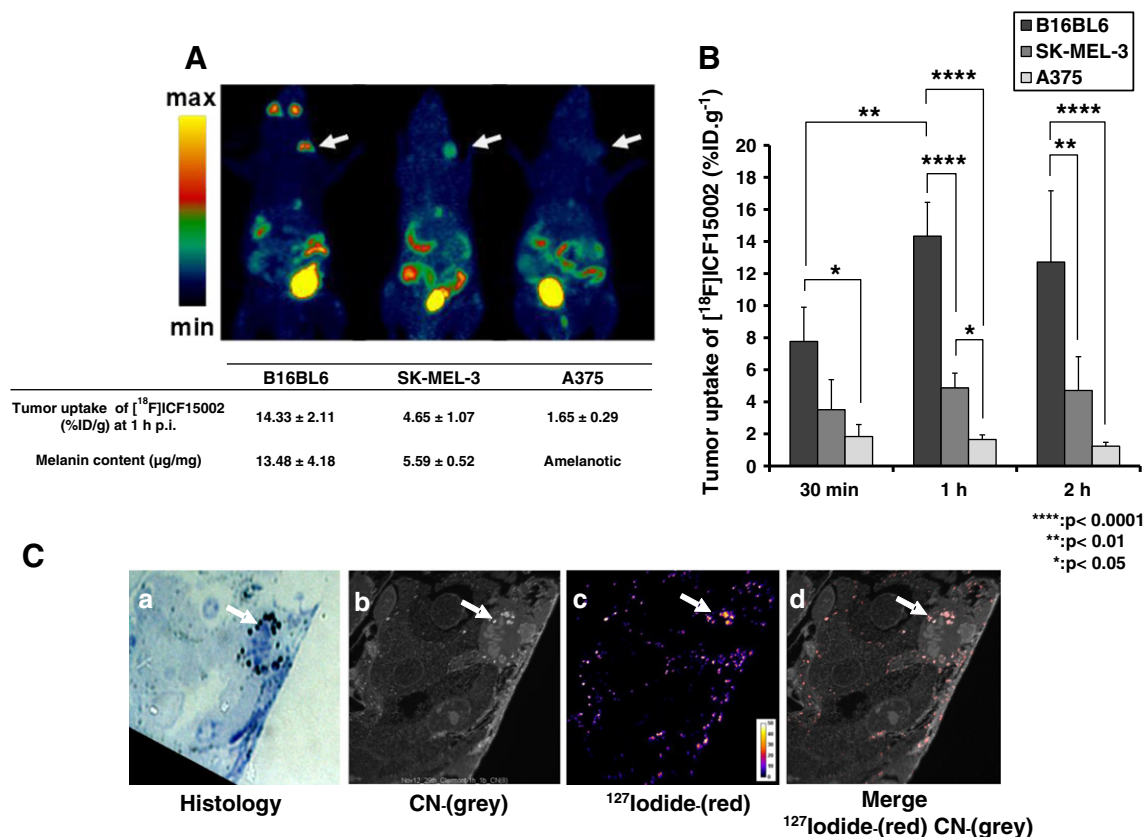
Figure 1. (A) Representative PET images of B16BL6, SK-MEL-3, and A375 bearing mice after [18F]ICF15002 injection (1 hour p.i.). (B) Quantitative analysis of PET (one-way ANOVA and Tukey *post hoc* test). (C) SIMS analysis (field of view: 50×50 μm) of B16BL6 lung colony after ICF15002 injection (0.1 μmol/mouse; 1 hour p.i.). (a) Histology with melanosomes identification, (b) $^{12}C^{14}N^{-}$ ions mapping, (c) $^{127}I^{-}$ ions mapping using fire LUT to display variations of iodine count. (d) Superimposition of the $^{12}C^{14}N$ and $^{127}I^{-}$ ion signals showing colocalization of ICF15002 and melanin signals.

antibody-antigen binding was detected by chemiluminescence using HRP-labeled second antibody (SouthernBiotech). Films were scanned using a calibrated BioRad GS 800 densitometer and analyzed by Quantity One software.

For flow cytometry analysis, B16BL6 tumors were mechanically disaggregated in PBS by fine mincing with 26G needles, filtered through a 70 μm nylon filter, and centrifuged (400 g, 8 minutes, 4°C), and dry pellets were stored in liquid nitrogen. After thawing, extracts were resuspended in ribonuclease A (500 μl, 1 mg/ml), and propidium iodide (500 μl, 0.1 mg/ml) was added. After 30 minutes at 4°C in the dark, cell cycle phases were gated manually using the BD-LSRII flow cytometer with FACSDiva Software (BD Biosciences) at 488/620 nm and analyzed with ModFit LT software (Verity Software House, Topsham).

Histology was performed on tumor and skin being cut in 4 μm slices and stained with hematoxylin-phloxin. An anti-PS100 antibody was used for hair follicle melanocyte staining. Whole eyes were cut in 5 μm slices and stained with hematoxylin-eosin-saffron. The thickness of the total retina outer and inner nuclear layers was measured both near to and remote from the optic nerve using metamorph software.

Absorbed doses to the tumor and major organs were determined from [125I]ICF15002 kinetic data using the Medical Internal Radiation Dose (MIRD) methodology. Final results were extrapolated to [131I]ICF15002 using the cumulative activity, the equilibrium

dose constant of iodine-131, the absorbed dose fractions, and the geometric volumes of organs and tumor [24].

Statistical Analysis

Statistics used GraphPad Prism6 software (GraphPad): two-tailed Student's *t* test for comparing means of two independent groups and one-way analysis of variance (ANOVA) and *post hoc* (Tukey, Dunnett, or Holm-Sidak) tests when multiple comparisons were needed. Correlation studies used Pearson correlation method. In TRT experiment, survival was assessed by the Kaplan-Meier method, and results were ranked according to the Mantel-Cox and log-rank test. The proportions of animals with metastasis were compared with Mann-Whitney test. $P < .05$ was considered statistically significant (*$P < .05$, **$P < .01$, ***$P < .001$, ****$P < .0001$).

Results

Radiochemistry

[131I]ICF15002 was obtained by radioiododemetallation from its stannane precursor in 120 minutes with 80% overall radiochemical yield (decay-corrected, RCY), a radiochemical purity (RCP) > 99% (Supplementary Figure 1, *A–C*), and specific activity of 99 to 130 GBq/μmol. According to the same procedure, [125I]ICF15002 was obtained in 120 minutes, with 83% overall RCY, an RCP > 99%,
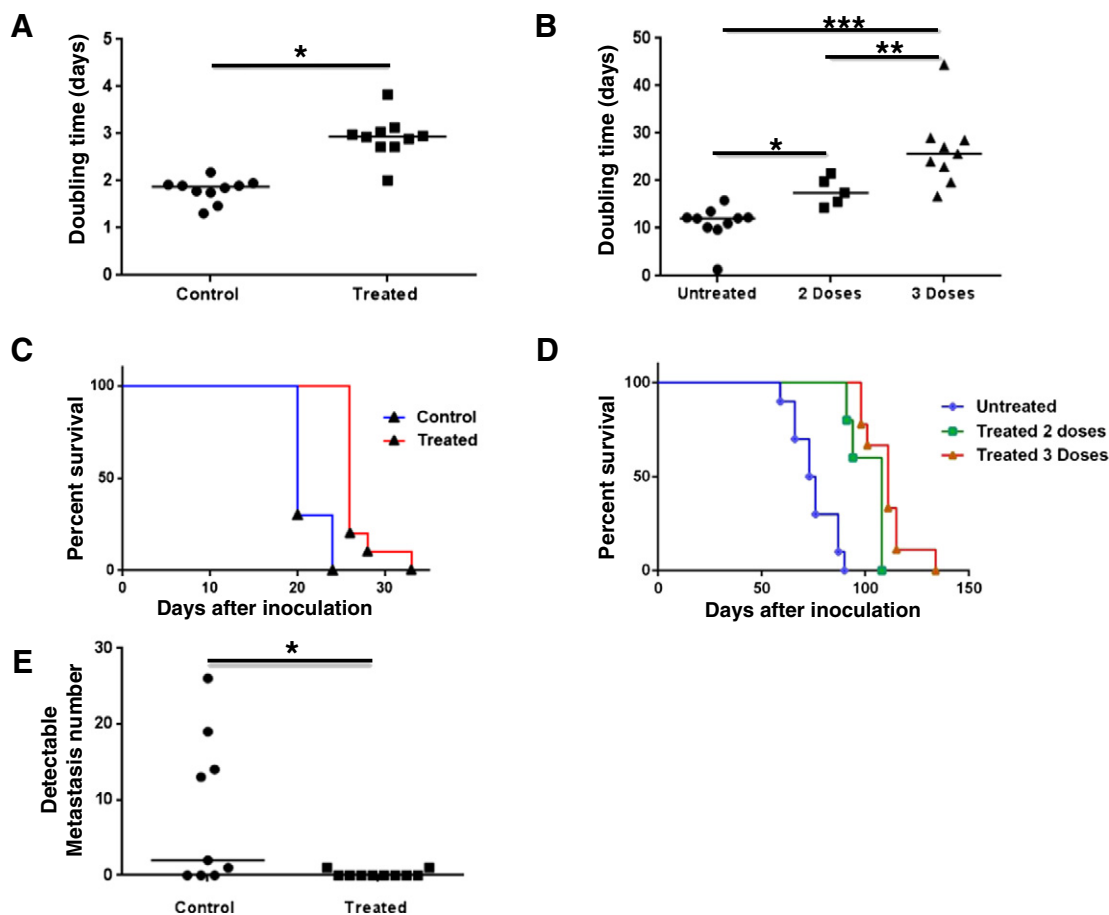
Figure 2. TRT with [131I]ICF15002 in B16BL6 and SK-MEL-3 models. (A) DTs for B16BL6 model (unpaired *t* test; P = .006). (B) DTs for SK-MEL-3 model (ANOVA and Holm-Sidak *post hoc* test; P < .0001). (C and D) Kaplan-Meier curves for B16BL6 and SK-MEL-3 models (Mantel-Cox test; log rank < .0001). (E) Spontaneous lung metastasis occurrence in B16BL6 model (Mann-Whitney; P = .0202).

and a specific activity of 107 to 121 GBq/μmol. [18F]ICF15002 was prepared as previously published [22] and obtained in 57 minutes, with 21% overall RCY (decay-corrected), an RCP > 99%, and a specific activity of 45 to 53 GBq/μmol. ICF15002 labeled by 125I, 131I, or 18F was radiochemically stable at room temperature in saline for at least 22 hours after preparation.

Distribution of [18F]ICF15002 by Both In Vivo PET Imaging and Ex Vivo Organ Counting

PET imaging results with [18F]ICF15002 were compared at 1 hour p.i. in melanoma models with different pigmentation status. Representative coronal images shown in Figure 1*A* revealed that tumors were clearly evidenced in both pigmented B16BL6 murine and SK-MEL-3 human xenografts. From quantitative analysis (Figure 1*B*), [18F]ICF15002 rapidly accumulated in pigmented tumors as early as 30 minutes p.i. (7.77 ± 2.13%ID/g and 3.51 ± 1.88%ID/g in B16BL6 and SK-MEL-3, respectively), reaching values of 14.33 ± 2.11%ID/g (B16BL6) and 4.65 ± 1.07%ID/g (SK-MEL-3) at 1 hour p.i. (P =.001) and remaining stable over 2 hours. The low accumulation of [18F]ICF15002 in muscles (1.4 ± 0.4%ID/g and 1.34 ± 0.42%ID/g, respectively, for B16BL6- and SK-MEL-3–bearing mice at 1 hour p.i.) led to a high-contrasted tumor imaging as early as 1 hour p.i. with tumor-to-muscle ratios being 11.0 ± 2.9 for B16BL6 and 4.09 ± 1.87 for SK-MEL-3 models. [18F]ICF15002 accumulation in A375

amelanotic xenografts was lower than 2%ID/g over 2 hours. These results supported a tracer accumulation in relation to tumor melanin content (r^2 = 0.98). For all animals, radioactivity was also evidenced in bladder and intestine as reflected by both urinary and fecal excretions. *In vivo* results were confirmed by *ex vivo* distribution (Supplementary Table 1), confirming the affinity of [18F]ICF15002 for pigmented tissues and melanoma, as well as its urinary and hepatobiliary elimination and its low defluorination over the 2 hours postinjection.

Intracellular Localization of ICF15002 in B16BL6 Melanoma

SIMS technique was used to determine intracellular localization of the compound ICF15002, with images centered on a B16BL6 melanoma pulmonary colony at 1 hour post intravenous injection (0.1 μmol/mouse). As illustrated in Figure 1*C*, superimposition of the $^{12}C^{14}N^-$ and $^{127}I^-$ signals indicated a perfect colocalization of $^{127}I^-$ signal of ICF15002 with melanin polymers in melanosomes.

[131I]ICF15002 TRT on Murine and Human Melanomas

In the highly pigmented B16BL6 model, two injections of [131I]ICF15002 (2 × 20 MBq) induced a significant (P = .006) inhibition of tumor growth with DT being 2.92 ± 0.45 days as compared with DT of 1.80 ± 0.25 days in controls (Figure 2*A* and Supplementary Figure 2). In SK-MEL-3 xenograft (Figure 2*B* and
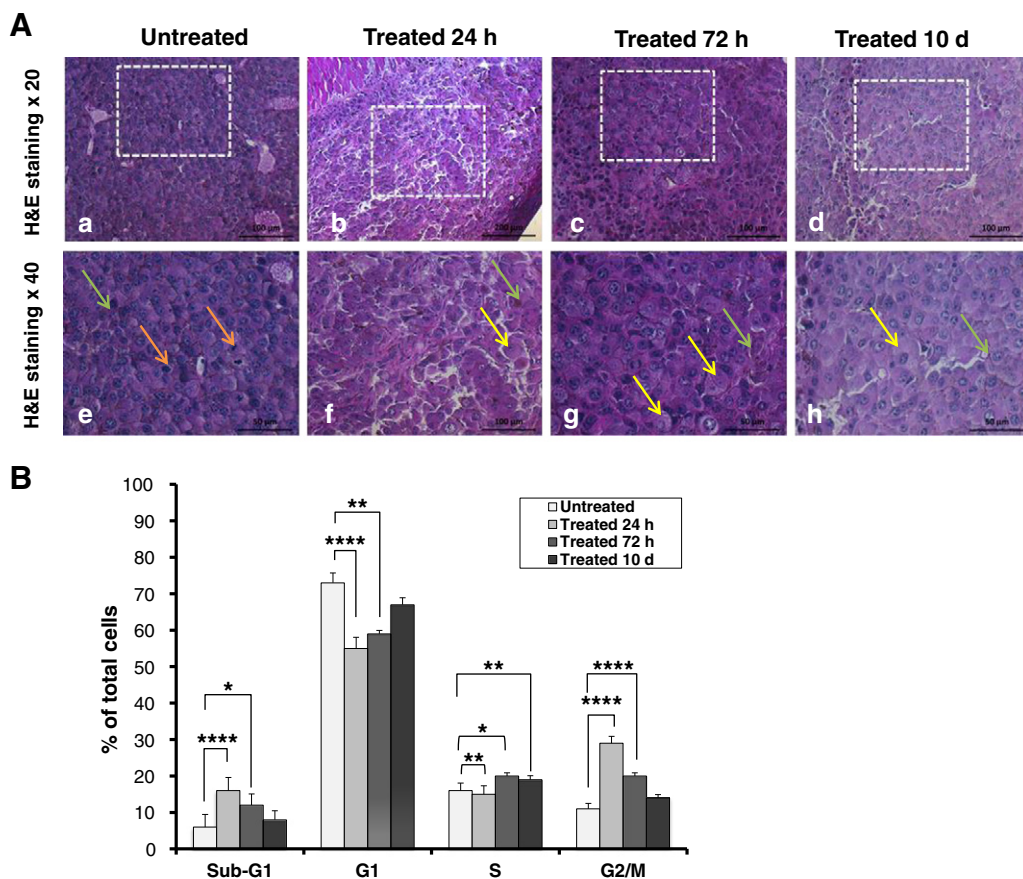
Figure 3. Mechanistic study of [^{131}I]ICF15002 TRT in B16BL6 model. (A) Histology of untreated tumors (a, e) showing mitosis (orange arrows) and treated tumors at 24 hours (b, f), 72 hours (c, g), and 10 days (d, h) p.i. Treated tumors evidenced anisocaryosis (yellow arrows) and abundant extracellular melanin deposits (green arrows) as early as 24 hours after TRT. (B) Cell cycle analysis of tumors at 24 hours and 72 hours p.i. and 10 days post-TRT (ANOVA and Tukey *post hoc* test *$P < .05$, **$P < .01$, ***$P < .001$, ****$P < .0001$). $n = 3$ controls and 5 treated.

Supplementary Figure 2), a significant inhibition of tumor growth was also observed after two injections of [^{131}I]ICF15002 (2 × 25 MBq) with DT of 17.75 ± 0.45 days versus 11.01 ± 3.81 days in controls ($P = .0393$). When SK-MEL-3–bearing mice were given three [^{131}I]ICF15002 doses (3 × 25 MBq), DT was 26.46 ± 7.85 days ($P < .0001$). The antitumor effect of TRT was associated with a lengthening of the treated-mice survival time in both B16BL6 model (27 days vs 21 in controls; $P < .0001$; Figure 2C) and SK-MEL-3 xenograft treated with two or three doses of [^{131}I]ICF15002 (108 days and 111 days, respectively, vs 74 days in controls; $P < .0001$) (Figure 2D). By day 95, 100% (10/10) of untreated SKMEL-3–bearing mice were sacrificed because of ethical end points. In contrast, 83% (5/6) of the two-dose group and 89% (8/9) of three-dose mice were still alive 95 days p.i. Metastasis number decrease occurred in B16BL6-treated group (Figure 2E): pulmonary nodules were observed in 6 of 9 controls mice, whereas only 1 very small nodule was detected in 2 of 10 treated animals ($P = .0202$). No decrease in body weight higher than 10% (data not shown) or signs of distress were observed with [^{131}I]ICF15002 treatment in either B16BL6 or SK-MEL-3 models.

Molecular Characterization of TRT in B16BL6 (Figures 3 and 4)
  [^{131}I]ICF15002 induced a decrease in mitotic index and vascularization as early as 24 hours after TRT (Figure 3A): treated

tumors exhibited atypia with anisocaryosis, two-fold lower mitotic index (around 10 mitoses per field in treated tumors vs 20 in controls) and a decrease in vascularization. It should be mentioned that extracellular melanin increase was observed with respect to controls at 24 hours, 72 hours, and 10 days. As illustrated in Figure 3B, flow cytometry analysis of tumor samples evidenced a significant increase in sub-G1 cell content 24 hours (+143%; $P < .0001$) and 72 hours posttreatment (+80%; $P < .05$), suggesting DNA fragmentation. A significant increase in cell accumulation in the G2/M phases was also observed at 24 hours p.i. (+117%; $P < .05$) and 72 hours p.i. (+64%; $P < .05$), indicating a retardation or an arrest of cell cycle. WB showed an increase in P53 phosphorylation at serine15 in treated tumors vs controls at 24 and 72 hours p.i. (Figure 4, A and B). P21 expression, a cyclin-dependent kinase inhibitor, was induced in treated tumors 24 hours, 72 hours, and 10 days p.i. (Figure 4, A and C). VEGF protein level was significantly decreased in treated mice at 72 hours p.i. (Figure 4D).

Absorbed Dose (Figures 5 and 6)
  Considering that [^{131}I]ICF15002 treatment modified tumor growth, biological half-life in the tumor was extrapolated by taking into account the TV changes after treatment. As shown in Figure 5A, absorbed dose to B16BL6 tumor was 102.3 Gy and lower than 5 Gy
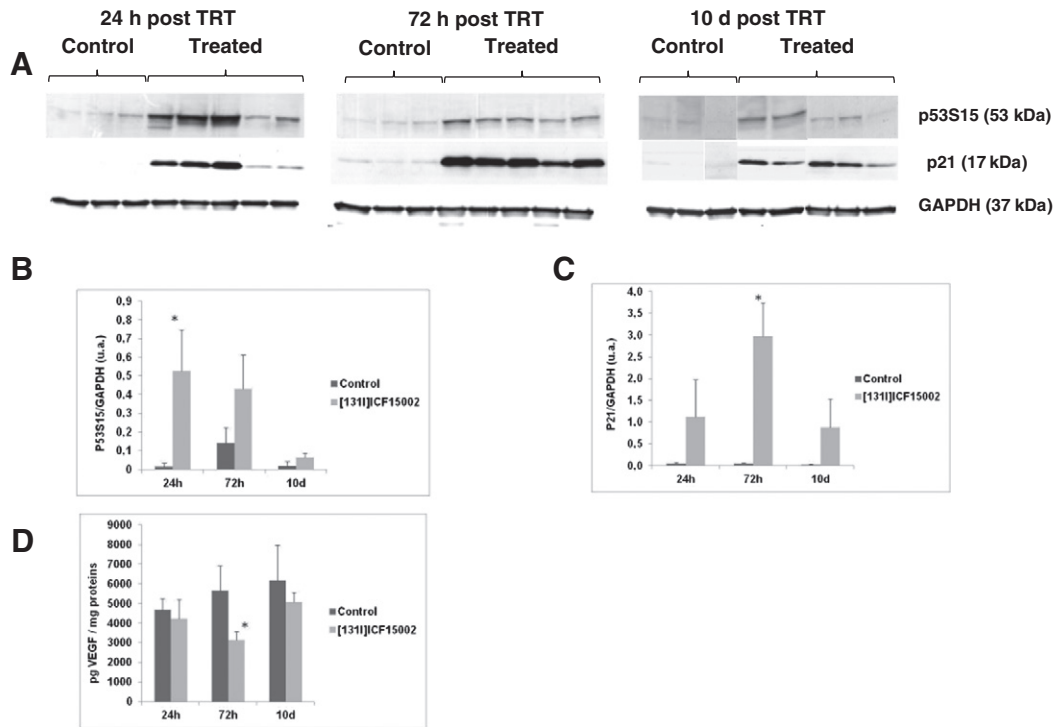
Figure 4. Mechanistic study of [^{131}I]ICF15002 TRT in B16BL6 model. (A) Western blot of tumors and quantitative analysis of p53S15 (B) and p21 expression (C) at 24 hours, 72 hours, and 10 days post-TRT (Student's t test, $P < .05$, $n = 3$ for controls, $n = 5$ for treated). (D) ELISA analysis of VEGF expression at 24 hours, 72 hours, and 10 days post-TRT (ANOVA and Dunnett test; $n = 3$ controls and $n = 5$ treated).

for nontarget organs, except for stomach (8.74 Gy) and highly pigmented eyes (83.04 Gy). Interestingly, in brain, which contains neuromelanin-containing neurons in the *substantia nigra*, absorbed dose was very low (0.24 Gy). Considering adverse effects (Figure 5, *B* and *C*), TRT induced a significant decrease in leukocyte number at 24 and 72 hours p.i. [^{131}I]ICF15002 TRT induced a decrease thickness of the outer layer of retina at ±0.8 mm from optical nerve. No significant effect was observed in the inner layer of retina thickness. No histological lesion and no changes in melanocyte number (one to two PS100-positive cells per field) were evidenced with respect to controls at 24 hours, 72 hours, and 10 days p.i. (Figure 6).

Excretion and Metabolism of [^{125}I]ICF15002

Excretion occurred *via* urinary and hepatobiliary systems, with 53% of radioactivity being recovered in the first 24 hours p.i. (28% in urine and 25% in feces). These percentages fell to 4% between 24 and 48 hours p.i (Supplementary Tables 2 and 3). In melanin-rich tissues (tumor, eyes), more than 90% of radioactivity corresponded to unchanged [^{125}I]ICF15002 at all time points. A fast breakdown of [^{125}I]ICF15002 was observed in excretion organs and biofluids (<4% in blood, 28% to 9% in liver, 13% to 0% in kidneys and urine between 1 and 6 hours p.i., and <5% in feces between 0 and 48 hours p.i.). Four metabolites were identified: [^{125}I]M4 was only found in the liver at 1 hour p.i. (8%) and in the feces between 0 and 48 hours p.i. (<7%). [^{125}I]M3 increased in the liver between 1 and 24 hours p.i. (26% to 71%) and decreased in the kidneys between 1 and 6 hours p.i. (19% to 0%). This metabolite was also found in urine and feces (<16% between 0 and 48 hours p.i.). [^{125}I]M2 was only detected in urine, with a decreasing percentage (30% to 0%)

between 1 and 72 hours p.i. [^{125}I]M1 percentage decreased in blood (22% to 11%) and increased in the kidneys (29% to 43%) between 1 and 6 hours. [^{125}I]M1 was also detected in urine and feces (<20% during the first 24 hours). These results led us to suggest the radiometabolic pathway presented in Figure 7.

Discussion

In this era of personalized medicine, both oncogene-targeted therapy and immune checkpoint blockade approaches have shown remarkable efficacy in a subset of patients with advanced metastatic melanoma. However, there is still a need for additional therapeutic options to increase disease-free survival of patients developing resistance [25,26]. Multitargeted upfront approach seems likely to yield the greatest survival benefit, and melanin-targeted radionuclide therapy (TRT) can be one option [27].

Both preclinical and clinical studies have demonstrated the interest of arylcarboxamide derivatives as small molecules that freely cross the cell membrane to bind to melanin, and provide high tumor-to-background background ratios. Particularly, ICF01012 developed by our group displayed highly specific and long-lasting uptake in the tumor, at the origin of promising antitumor efficacy in xenograft models [18,28].

For TRT applications, it is of high priority to stratify patients. This is particularly of interest for metastatic melanoma to identify patients eligible for melanin-TRT approach because pigmentation differs between metastases and primary lesions [15]. This prompted us to investigate a "theranostic" strategy by using iodinated and fluorinated matched-pair radiotracers offering both diagnosis *via* SPECT with iodine-123 and PET imaging (fluorine-18), and therapy (with iodine-131).
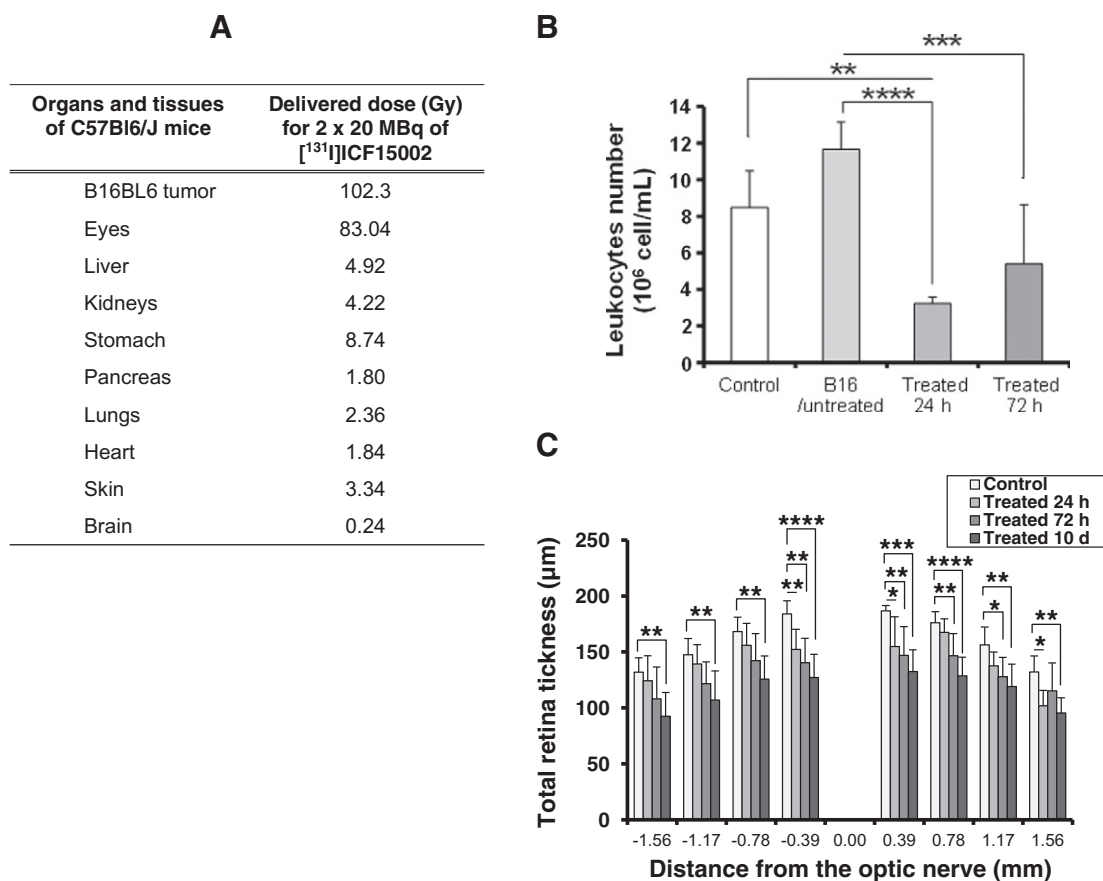
A

Organs and tissues of C57Bl6/J mice	Delivered dose (Gy) for 2 x 20 MBq of [131I]ICF15002
B16BL6 tumor	102.3
Eyes	83.04
Liver	4.92
Kidneys	4.22
Stomach	8.74
Pancreas	1.80
Lungs	2.36
Heart	1.84
Skin	3.34
Brain	0.24

Figure 5. Absorbed dose and side effect in B16BL6 model. (A) Dose calculations with MIRD (obtained from *ex vivo* biodistribution of [125I]ICF15002 and extrapolated for [131I]ICF15002). (B) TRT effect on leucocytes number (n = 4-5 animals/time point) (ANOVA and Dunnett *post hoc* test *P < .05, **P < .01, ***P < .0001). (C) TRT effect on total retina thickness at 24 hours, 72 hours, and 10 days (different distances from optical nerve presented).

ICF15002 was firstly selected as a good candidate from a series of arylcarboxamide derivatives on the basis of its radiochemical properties and physicochemical properties [21,22]. This preclinical work highlights the interest of ICF15002, when radiolabeled either with fluorine-18 or iodine-131, for a theranostic management of melanoma. First of all, biodistribution of [18F]ICF15002 was characterized in murine and human melanoma models by both *in vivo* PET imaging and *ex vivo* biodistributions. As expected, biodistribution studies in melanoma-bearing mice demonstrated an early and high tumor accumulation of [18F]ICF15002, as early as 30 minutes p.i., correlated to pigmentation (r^2 = 0.98) and leading to high and durable tumor-to-muscle ratios (12.12 ± 1.74 for B16BL6 and 4.23 ± 1.11 for SK-MEL-3 at 1 hour p.i.). It should be mentioned that [18F]ICF15002 uptake in the eyes of the animals differs between the two mouse models showing specificity of targeting: a high uptake was observed in the highly pigmented eyes of C57BL/6J mice, whereas a low pattern was observed in the amelanotic eyes of nude mice. This is consistent with the ability of ICF15002 to bind to melanin *in vivo*. The specific affinity of ICF15002 for melanin was confirmed at the cellular level by SIMS analysis of pulmonary melanoma micronodules: a colocalization of the iodine signal of ICF15002 with that of melanin was clearly evidenced in tumor cell melanosomes.

The therapeutic potential of [131I]ICF15002 was firstly assessed and extensively characterized in the highly pigmented B16BL6 murine model: for two injections of [131I]ICF15002 (20 MBq/dose), absorbed doses in tumor were estimated at 102.3 Gy. This dose induced tumor growth inhibition with DTs of 2.92 ± 0.45 days in treated group as compared with 1.80 ± 0.25 days in controls. TRT was associated with an early increase in both G2/M and sub-G1 blockage, with the induction of P53S15 phosphorylation leading to P21 expression and to cell death, as observed for similar TRT approaches [19,29]. P21 expression is known to be dependent of P53 transcriptional activation, and both P21 and P53 control the G1/S and G2/M cell cycle checkpoints. It should be underlined that TRT with [131I]ICF15002 interestingly reduced metastatic spread from the primary tumors. At later stages of TRT, VEGF downregulation and extracellular melanin increase were also evidenced. Such extracellular melanin release may be considered as an additional target for a second TRT round [19,30,31].

Considering that B16BL6 model is highly pigmented, we assessed the potential of [131I]ICF15002 for TRT in the lower pigmented human SK-MEL-3 model: the antitumor efficacy was still observed with DT being increased by a factor of 1.5 and 2.3 for two and three doses, respectively.

In view of potential clinical applications, metabolism and dosimetry to nontarget organs have also to be considered. *In vivo*
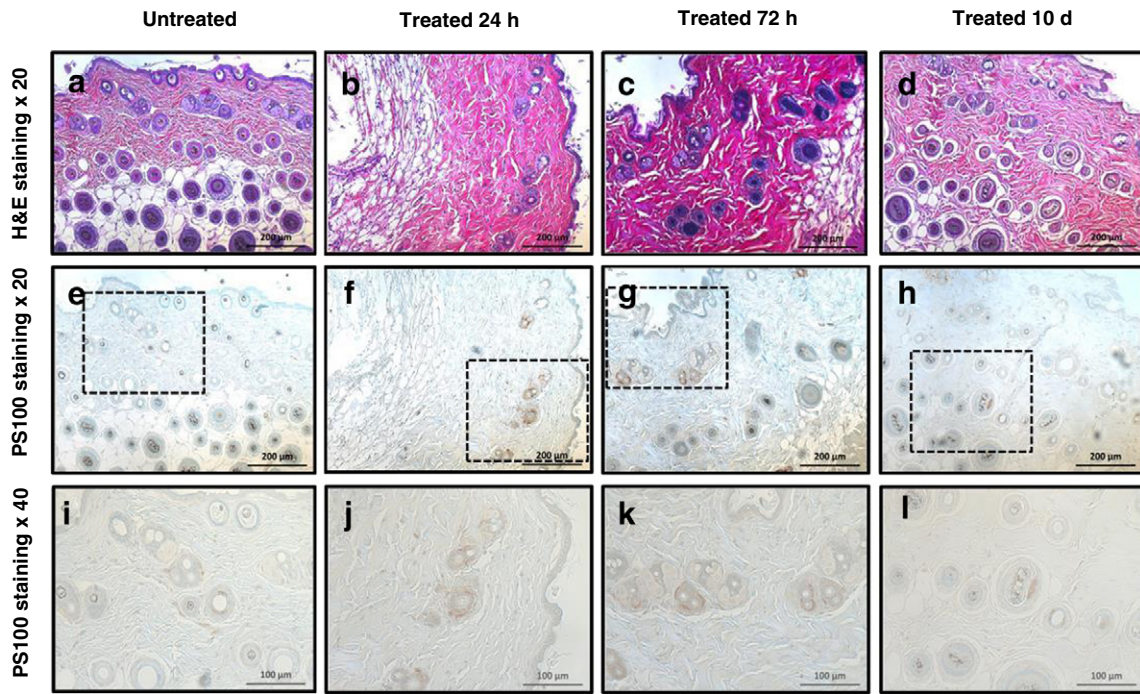
Figure 6. Skin histology in B16BL6-bearing mice at 24 hours, 72 hours, and 10 days of protocol. HES (×200) and PS100 (×20 and ×40) staining is presented.

metabolism of ICF15002 was determined in B16BL6 model after radiolabeling by iodine-125. A high stability in melanin-rich tissues (such as tumor and highly pigmented eyes) was observed with about 90% of the radioactive signal corresponding to the unchanged [^{125}I]ICF15002 from 1 hour to 10 days p.i. Excretion of [^{125}I]ICF15002 was mainly attributable to dealkylation and hydrolysis, leading thus to four main radiolabeled identified

metabolites. Regarding dosimetry, for a protocol of 2 × 20 MBq of [^{131}I]ICF15002 at 4-day interval, absorbed dose was lower than 5 Gy for most organs of the animals, including skin and brain which contain pigmented cells. The absorbed dose delivered to black mice's eyes of the B16BL6 model was estimated to be 83.04 Gy. Histology evidenced a 30% mean decrease of the outer layer thickness of retina being localized at ± 0.80 mm from optical nerve, with no lesions
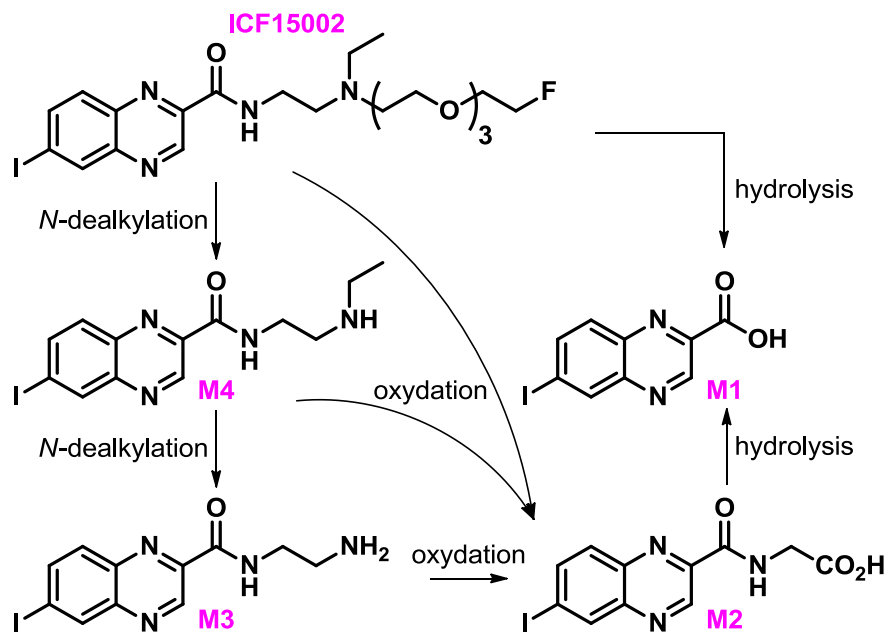

Figure 7. Proposal of *in vivo* metabolism pathways of [^{125}I]ICF15002.

observed in the inner layer of retina. Because of many differences in melanin content, ocular geometry, and also ratio of the range of iodine-131 beta emission, respectively, to the size of eye [32,33], results obtained in C57BL6 mice's eyes should not be considered as predictive for human ones. In the clinical imaging study with [^{123}I]BZA2, no significant uveal uptake was indeed visualized on the human eyes except in the case of ocular melanoma, whereas great uveal uptake was observed in the mouse model [15]. Melanin-targeting agents such as [^{131}I]MIP1145 have previously been reported to highly accumulate in the pigmented eyes of C57BL6 mice (>30%ID/g) but to a lower extent in primates, with the highest delivered dose being only 6.8 Gy for a 3.7 GBq injection [17]. According to us, because of murine and human differences in ocular geometry and melanin content, [^{131}I]ICF15002 accumulation in black mice will not be transposable to human ones and should not be considered as a major problem for clinical transfer of this theranostic approach.

It is also important to note that the safety of melanin-TRT was recently demonstrated to be associated with a clinical benefit with the benzamide [^{131}I]IBA52 at therapeutic doses up to 3.9 ± 2.0 GBq in patients with metastatic melanoma [20]. In retina, absorbed doses were only 2.7 Gy/GBq vs 5.5 ± 3.6 Gy/GBq in melanoma metastases, and no retinopathies were observed [20].

In conclusion, our preclinical results demonstrate the potential of a unique iodinated and fluorinated scaffold for the theranostic management of pigmented metastatic melanoma.

Conflict of Interest

Authors declare that they have no conflict of interest.

Ethical Approval

All applicable international, national, and/or institutional guidelines for the care and use of animals were followed in accordance the European Directive 2010/63/UE.

Supplementary data to this article can be found online at http://dx.doi.org/10.1016/j.neo.2016.11.001.

References

[1] Finn L, Markovic SN, and Joseph RW (2012). Therapy for metastatic melanoma: the past, present, and future. *BMC Med* **10**, 23.

[2] Michielin O and Hoeller C (2015). Gaining momentum: New options and opportunities for the treatment of advanced melanoma. *Cancer Treat Rev* **41**, 660–670.

[3] Zhu Z, Liu W, and Gotlieb V (2016). The rapidly evolving therapies for advanced melanoma—towards immunotherapy, molecular targeted therapy, and beyond. *Crit Rev Oncol Hematol* **99**, 91–99.

[4] Redman JM, Gibney GT, and Atkins MB (2016). Advances in immunotherapy for melanoma. *BMC Med* **14**, 20.

[5] Robert C, Thomas L, Bondarenko I, O'Day S, Weber J, Garbe C, Lebbe C, Baurain JF, Testori A, and Grob JJ, et al (2011). Ipilimumab plus dacarbazine for previously untreated metastatic melanoma. *N Engl J Med* **364**, 2517–2526.

[6] Chapman PB, Hauschild A, Robert C, Haanen JB, Ascierto P, Larkin J, Dummer R, Garbe C, Testori A, and Maio M, et al (2011). Improved survival with vemurafenib in melanoma with BRAF V600E mutation. *N Engl J Med* **364**, 2507–2516.

[7] Riveiro-Falkenbach E, Villanueva CA, Garrido MC, Ruano Y, García-Martín RM, Godoy E, Ortiz-Romero PL, Ríos-Martín JJ, Santos-Briz A, and Rodríguez-Peralto JL (2015). Intra- and inter-tumoral homogeneity of BRAF(V600E) mutations in melanoma tumors. *J Invest Dermatol* **135**, 3078–3085.

[8] Boyd KP, Vincent B, Andea A, Conry RM, and Hughey LC (2012). Nonmalignant cutaneous findings associated with vemurafenib use in patients with metastatic melanoma. *J Am Acad Dermatol* **67**, 1375–1379.

[9] Hauschild A, Grob J-J, Demidov LV, Jouary T, Gutzmer R, Millward M, Rutkowski P, Blank CU, Miller Jr WH, and Kaempgen E, et al (2012). Dabrafenib in BRAF-mutated metastatic melanoma: a multicentre, open-label, phase 3 randomised controlled trial. *Lancet* **380**, 358–365.

[10] Lacouture ME, Duvic M, Hauschild A, Prieto VG, Robert C, Schadendorf D, Kim CC, McCormack CJ, Myskowski PL, and Spleiss O, et al (2013). Analysis of dermatologic events in vemurafenib-treated patients with melanoma. *Oncologist* **18**, 314–322.

[11] Eisenhut M, Hull WE, Mohammed A, Mier W, Lay D, Just W, Gorgas K, Lehmann WD, and Haberkorn U (2000). Radioiodinated N-(2-diethylaminoethyl)benzamide derivatives with high melanoma uptake: structure-affinity relationships, metabolic fate, and intracellular localization. *J Med Chem* **43**, 3913–3922.

[12] Chezal J-M, Papon J, Labarre P, Lartigue C, Galmier M-J, Decombat C, Chavignon O, Maublant J, Teulade JC, and Madelmont JC, et al (2008). Evaluation of radiolabeled (hetero)aromatic analogues of N-(2-diethylaminoethyl)-4-iodobenzamide for imaging and targeted radionuclide therapy of melanoma. *J Med Chem* **51**, 3133–3144.

[13] Michelot JM, Moreau MF, Veyre AJ, Bonafous JF, Bacin FJ, Madelmont JC, Bussiere F, Souteyrand PA, Mauclaire LP, and Chossat FM, et al (1993). Phase II scintigraphic clinical trial of malignant melanoma and metastases with iodine-123-N-(2-diethylaminoethyl 4-iodobenzamide). *J Nucl Med* **34**, 1260–1266.

[14] Moins N, D'Incan M, Bonafous J, Bacin F, Labarre P, Moreau M-F, Mestas D, Noirault E, Chossat F, and Berthommier E, et al (2002). 123I-N-(2-diethyla-minoethyl)-2-iodobenzamide: a potential imaging agent for cutaneous melanoma staging. *Eur J Nucl Med Mol Imaging* **29**, 1478–1484.

[15] Cachin F, Miot-Noirault E, Gillet B, Isnardi V, Labeille B, Payoux P, Meyer N, Cammilleri S, Gaudy C, and Razzouk-Cadet M, et al (2014). (123)I-BZA2 as a melanin-targeted radiotracer for the identification of melanoma metastases: results and perspectives of a multicenter phase III clinical trial. *J Nucl Med* **55**, 15–22.

[16] Rbah-Vidal L, Vidal A, Besse S, Cachin F, Bonnet M, Audin L, Askienazy S, Dollé F, Degoul F, and Miot-Noirault E, et al (2012). Early detection and longitudinal monitoring of experimental primary and disseminated melanoma using [^{18}F]ICF01006, a highly promising melanoma PET tracer. *Eur J Nucl Med Mol Imaging* **39**, 1449–1461.

[17] Joyal JL, Barrett JA, Marquis JC, Chen J, Hillier SM, Maresca KP, Boyd M, Gage K, Nimmagadda S, and Kronauge JF, et al (2010). Preclinical evaluation of an 131I-labeled benzamide for targeted radiotherapy of metastatic melanoma. *Cancer Res* **70**, 4045–4053.

[18] Bonnet M, Mishellany F, Papon J, Cayre A, Penault-Llorca F, Madelmont JC, Miot-Noirault E, Chezal JM, and Moins N (2010). Anti-melanoma efficacy of internal radionuclide therapy in relation to melanin target distribution. *Pigment Cell Melanoma Res* **23**, e1–11.

[19] Degoul F, Borel M, Jacquemot N, Besse S, Communal Y, Mishellany F, Papon J, Penault-Llorca F, Donnarieix D, and Doly M, et al (2013). In vivo efficacy of melanoma internal radionuclide therapy with a 131I-labelled melanin-targeting heteroarylcarboxamide molecule. *Int J Cancer* **133**, 1042–1053.

[20] Mier W, Kratochwil C, Hassel JC, Giesel FL, Beijer B, Babich JW, Friebe M, Eisenhut M, Enk A, and Haberkorn U (2014). Radiopharmaceutical therapy of patients with metastasized melanoma with the melanin-binding benzamide 131I-BA52. *J Nucl Med* **55**, 9–14.

[21] Maisonial A, Billaud EMF, Besse S, Rbah-Vidal L, Papon J, Audin L, Bayle M, Galmier MJ, Tarrit S, and Borel M, et al (2013). Synthesis, radioiodination and in vivo screening of novel potent iodinated and fluorinated radiotracers as melanoma imaging and therapeutic probes. *Eur J Med Chem* **63**, 840–853.

[22] Billaud EMF, Rbah-Vidal L, Vidal A, Besse S, Tarrit S, Askienazy S, Maisonial A, Moins N, Madelmont JC, and Miot-Noirault E, et al (2013). Synthesis, radiofluorination, and in vivo evaluation of novel fluorinated and iodinated radiotracers for PET imaging and targeted radionuclide therapy of melanoma. *J Med Chem* **56**, 8455–8467.

[23] Denoyer D, Labarre P, Papon J, Miot-Noirault E, Galmier M-J, Madelmont J-C, Chezal JM, and Moins N (2008). Development of a high-performance liquid chromatographic method for the determination of a new potent radioiodinated melanoma imaging and therapeutic agent. *J Chromatogr B Analyt Technol Biomed Life Sci* **875**, 411–418.

[24] Perrot Y, Degoul F, Auzeloux P, Bonnet M, Cachin F, Chezal JM, Donnarieix D, Labarre P, Moins N, and Papon J, et al (2014). Internal dosimetry through GATE simulations of preclinical radiotherapy using a melanin-targeting ligand. *Phys Med Biol* **59**, 2183–2198.

[25] Villanueva J, Vultur A, Lee JT, Somasundaram R, Fukunaga-Kalabis M, Cipolla AK, Wubbenhorst B, Xu X, Gimotty PA, and Kee D, et al (2010). Acquired resistance to BRAF inhibitors mediated by a RAF kinase switch in melanoma can be overcome by cotargeting MEK and IGF-1R/PI3K. *Cancer Cell* **18**, 683–695.

[26] Smalley KSM, Eroglu Z, and Sondak VK (2016). Combination therapies for melanoma: a new standard of care? *Am J Clin Dermatol* **17**, 99–105.

[27] Norain A and Dadachova E (2016). Targeted radionuclide therapy of melanoma. *Semin Nucl Med* **46**, 250–259.

[28] Viallard C, Perrot Y, Boudhraa Z, Jouberton E, Miot-Noirault E, Bonnet M, Mishellany F, Cayre A, Maigne L, and Rbah-Vidal L, et al (2015). [^{123}I]ICF01012 melanoma imaging and [^{131}I]ICF01012 dosimetry allow adapted internal targeted radiotherapy in preclinical melanoma models. *Eur J Dermatol* **25**, 29–35.

[29] Viallard C, Chezal J-M, Mishellany F, Ranchon-Cole I, Pereira B, Herbette A, Besse S, Boudhraa Z, Jacquemot N, and Cayre A, et al (2016). Targeting DNA repair by coDbait enhances melanoma targeted radionuclide therapy. *Oncotarget* **7**, 12927–12936.

[30] Bonnet-Duquennoy M, Papon J, Mishellany F, Labarre P, Guerquin-Kern J-L, Wu T-D, Gardette M, Maublant J, Penault-Llorca F, and Miot-Noirault E, et al (2009). Targeted radionuclide therapy of melanoma: anti-tumoural efficacy studies of a new 131I labelled potential agent. *Int J Cancer* **125**, 708–716.

[31] Thompson S, Ballard B, Jiang Z, Revskaya E, Sisay N, Miller WH, Cutler CS, Dadachova E, and Francesconi LC (2014). 166Ho and 90Y labeled 6D2 monoclonal antibody for targeted radiotherapy of melanoma: comparison with 188Re radiolabel. *Nucl Med Biol* **41**, 276–281.

[32] Durairaj C, Chastain JE, and Kompella UB (2012). Intraocular distribution of melanin in human, monkey, rabbit, minipig and dog eyes. *Exp Eye Res* **98**, 23–27.

[33] Dimasi DP, Hewitt AW, Kagame K, Ruvama S, Tindyebwa L, Llamas B, Kirk KA, Mitchell P, Burdon KP, and Craig JE (2011). Ethnic and mouse strain differences in central corneal thickness and association with pigmentation phenotype. *PLoS One* **6**, e22103.